Journal of the Mechanics and Physics of Solids 134 (2020) 103751

Contents lists available at ScienceDirect

Journal of the Mechanics and Physics of Solids

journal homepage: www.elsevier.com/locate/jmps

Fatigue-Resistant elastomers

Chenghai Li[a,1], Hang Yang[a,1], Zhigang Suo[b,*], Jingda Tang[a,*]

[a] State Key Lab for Strength and Vibration of Mechanical Structures, International Center for Applied Mechanics, Department of Engineering Mechanics, Xi'an Jiaotong University, Xi'an 710049, China
[b] John A. Paulson School of Engineering and Applied Science, Kavli Institute for Bionano Science and Technology, Harvard University, Cambridge, MA 02138, USA

ARTICLE INFO

Article history:
Received 11 August 2019
Revised 4 October 2019
Accepted 5 October 2019
Available online 6 October 2019

Keywords:
Elastomer
Fatigue-resistant
Threshold
3D printing
Composites

ABSTRACT

The resistance of a material to the growth of a crack is characterized by fracture toughness under monotonic load, and by fatigue threshold under cyclic load. The fatigue threshold of engineering elastomers is commonly limited to $\sim 50\,J/m^2$, much below their toughness ($10^3 \sim 10^5\,J/m^2$). Here we report fatigue-resistant elastomers with threshold beyond $500\,J/m^2$. Such an elastomer is a composite of two elastomers: a lattice of a hard elastomer embedded in a matrix of soft elastomer. Both the hard and soft elastomers are elastically stretchable, with small hysteresis. At a crack front in the composite, the soft matrix shears greatly, which de-concentrates stress in the hard lattice. When the crack advances in the composite, the energy dissipated scales with the feature size of the lattice. By contrast, when a crack advances in a homogeneous elastomer, the energy dissipated scales with the mesh size of the polymer network. The fatigue-resistant elastomers open new opportunities for applications requiring stretchable materials.

1. Introduction

Elastomers are ubiquitous in daily life, engineering, and medicine (Bhowmick and Stephens, 2000; Gent, 2012). Examples include balloons (Merritt and Weinhaus, 1978), car tires (Takeyama and Matsui, 1969), tubes (Zhu et al., 2010), seals (Le Floch et al., 2018; Whanger and Harrall, 2004), gloves (Wiley, 1934), footballs (Martin, 1959), soft robots (Ilievski et al., 2011; Shepherd et al., 2011), and stretchable electronics (Kim et al., 2011; Mannsfeld et al., 2010; Rogers et al., 2010; Yang and Suo, 2018; Yang et al., 2019b). Since the 1950s, the fracture of elastomers has been extensively studied; See recent reviews (Creton and Ciccotti, 2016; Long and Hui, 2015; Mars and Fatemi, 2002). Elastomers are made of entropic polymer networks, capable of repeated and large deformation. Lake and Thomas noted that the fatigue threshold for various elastomers is about $\Gamma_0 = 50\,J/m^2$ (Lake and Thomas, 1967), much below their toughness ($10^3 \sim 10^5\,J/m^2$). Lake and Thomas argued that, when a crack advances near the threshold, the low amplitude of cyclic load will not activate any energy dissipation in the bulk of the elastomer, so that the threshold comes from the energy dissipated in breaking the polymer chains lying on the crack plane. The Lake-Thomas model explains the low threshold of elastomers. Since then, how to enhance the fatigue threshold of elastomers has become a long standing issue. A conflict exists: a polymer network of long chains has high threshold, but low stiffness (Bhowmick, 1988).

* Corresponding authors.
E-mail addresses: suo@seas.harvard.edu (Z. Suo), tangjd@mail.xjtu.edu.cn (J. Tang).
[1] These authors contributed equally to this work.

https://doi.org/10.1016/j.jmps.2019.103751
0022-5096/

Nature has discovered a strategy to resist fatigue crack. Skins, muscles, bones and cartilages use microstructures to deflect cracks (Berisio et al., 2002; Jurvelin et al., 2003; Launey et al., 2010; Ritchie, 2014; Wegst et al., 2015; Yang et al., 2015). Crack deflection makes polyvinyl alcohol (PVA) hydrogels insensitive to flaws under both monotonic and cyclic loads (Bai et al., 2019b). High threshold beyond 1000 J/m^2 has been reported (Lin et al., 2019a, 2019b). The aligned PVA polymer chains in the crystalline domain resist the crack growth, and the rupture of a bundle of chains will release a lot of energy, which improves the threshold. However, the crystalline chains are only specific to limited types of polymers. It has been proposed to synthesize fatigue-resistant stretchable materials by embedding stretchable hard fibers inside a soft matrix (Wang et al., 2019; Xiang et al., 2019). The great shear in the soft matrix will alleviate the stress concentration in the hard fibers at the crack front. The crack is first blocked by the hard fiber; once the crack cuts the fiber, a large amount of elastic energy stored in the fiber will be released. Through this design, a threshold above 1000 J/m^2 has been achieved using fibers of a polydimethylsiloxane (PDMS) (Xiang et al., 2019). However, the PDMS fibers are not quite stretchable (ultimate stretch <2) and the one-dimensional (1D) aligned fibers can only resist the fatigue crack in one direction. To reinforce materials in multiple directions, it is necessary to embed two-dimensional (2D) or even three-dimensional (3D) lattice inside a soft matrix. Lattices here mean the layout of the fibers: the macroscopic regular 2D patterns or 3D structures.

Here we report composite elastomers with high threshold ($>$500 J/m^2), high toughness ($>$6000 J/m^2), and high stretchability (>5). The composite elastomer consists of an elastomer lattice with a high modulus (hard elastomer) and elastomer matrix with a low modulus (soft elastomer). We describe methods of fabrication and mechanical tests (Section 2). We compare the available data of threshold and toughness of various elastomers (Section 3). As a crack advances in the composite, the energy dissipated scales with the length of fibers. Since the energy stored in a macroscopic fiber is much higher than that of polymer chains, the fatigue threshold can be markedly enhanced (Section 4). We use the extrusion printing to embed 2D hard elastomer structures (square and honeycomb) in the soft elastomer (Section 5). The high modulus contrast and the strong interface adhesion between the hard and soft elastomers enable the fatigue resistance of the composite (Section 6). We compare the fracture process of the 1D fiber and 2D structure reinforced composites and find that 2D composites are better than 1D composites in terms of preventing crack kinking (Section 7). We describe the observed failure modes in the fatigue test of 2D composites. We further plot a curve of the energy release rate versus cycle number (G-N curve). The composite shows a high threshold beyond 500 J/m^2 (Section 8).

2. Experimental section

2.1. Synthesis of homogenous elastomers

We used two commercial silicone elastomers in our experiments: Ecoflex-0030 and Dragon skin-0020 from Smooth-On, Inc, both are platinum-catalyzed elastomers by mixing two parts (Part A and Part B). The polymerization process can be understood as following: catalyzed by platinum, the -SiH groups of the crosslinkers can react with the vinyl groups on the polymer chain to form three dimensional networks (Liu et al., 2018). Part A and Part B of Ecoflex-0030 were mixed with 1:1 wt ratio to prepare the soft elastomer. Dragon skin-0020 A and Ecoflex-0030 B were mixed in various weight ratios (1:1.5, 1:1.75 and 1:2) to synthesize hard elastomers. Part A and Part B were transferred to a vessel and mixed by a planetary mixer (Thinky ARE-300) at 2000 RPM for one minute and degassed at 2200 RPM for another one minute. Then the precursor was poured into a glass mold with a spacer made of silicone rubber (thickness, 1 mm). The sample was stored in an oven at 60 °C for 4 h to cure the elastomers completely.

2.2. Manufacture of composite elastomers

The composite elastomers consisted of two constituents: the hard elastomer and the soft elastomer. For all the manufacture of composite elastomers, we used the weight ratio of (A:B = 1:1.5) to prepare the hard elastomer because it showed the highest modulus. Dragon skin-0020 A and Ecoflex-0030 B were first mixed by a planetary mixer and then loaded into a syringe of a 3D printer. The printer was modified from a MakerBot Replicator 2X. An air bump system (OTS-800-30L and AD-982) was set up to extrude the ink. Meanwhile, the metal platform of the printer was pre-heated to 110 °C. Driven by the air pressure, the precursor flowed from the nozzle to the platform in a designed pattern. The hot platform initiated the fast polymerization of the hard elastomer. After printing, the patterned hard elastomer was stored in an oven at 60 °C for 4 h to complete the polymerization. Next, the precursor of the soft elastomer was infused into the mold to fill the space left by the hard elastomer pattern. The composite was then stored at room temperature for 12 h for the polymerization of the soft matrix.

For the 2D square composite, the average width w_f and thickness t_f of a single fiber were 3.4 mm and 1.8 mm, respectively. The average spacing S_f between two fibers was 8.9 mm. The thickness of the soft matrix t_m was 0.9 mm. For the 2D honeycomb composite, the average width w_f and thickness t_f of a single fiber were 3.2 mm and 1.8 mm, respectively. The average side length of the internal hexagon S_f was 5.0 mm. The thickness of the soft matrix t_m was 1.3 mm. For the 1D fiber composite, the average width w_f and thickness t_f of a single 1D fiber were 3.2 mm and 1.8 mm, respectively. The average spacing S_f between two 1D fibers was 9.6 mm. The thickness of the soft matrix t_m was 1.26 mm.

2.3. Mechanical measurements

All mechanical measurements, including uniaxial tension, pure-shear test, 180-degree peeling test and fatigue test, were performed with a tensile machine (SMADAZU AGS-X). All specimens were loaded at a velocity of 50 mm/min except for the fatigue test. The fatigue test was loaded at a frequency of $f = 0.2$ Hz. An initial cut of 20 mm was set for the pure-shear and fatigue tests.

For uniaxial tension and peeling test, the length and width refer to the sample sizes parallel and perpendicular to the loading direction, respectively. For pure-shear and fatigue test, the height and width refer to the sample sizes parallel and perpendicular to the loading direction, respectively.

For uniaxial tension, the sample was cut into a dumbbell shape (length = 12 mm, width = 2 mm) using a designed metal cutter. For pure-shear tests, the sample was cut into 20 mm or 40 mm in height and 100 mm in width using a designed metal cutter.

For 180-degree peeling samples, the hard elastomer was first fully cured with a size of 80 mm × 10 mm × 2 mm. The hard rubber was transferred into a mold of 80 mm × 10 mm × 3 mm, and a piece of paper with a size of 10 mm × 10 mm was attached to one end of the hard rubber to introduce an initial crack. Then the precursor of the soft elastomer was poured into the mold with a thickness of 1 mm. The whole sample was then put into an oven at 60 °C for 4 h to complete the polymerization of the soft rubber and formed strong interface adhesion. To constrain the deformation of the peeling arms in the tests, stiff PET backings with a size of 80 mm × 12 mm × 0.05 mm were glued to back sides of both the hard elastomer and soft elastomer. The glue we used is a commercial product (Ausbond RTV adhesive).

The sample size for uniaxial tension was 12 mm × 2 mm × 1 mm. The Young's modulus was calculated by the linear fitting of the uniaxial tension curve from $\lambda = 1$ to $\lambda = 2.5$. The sample size for the pure-shear test was 20 mm × 100 mm × 1 mm. Stretch λ (also called extension ratio) is defined as the current size dividing by the initial size of a specimen in the loading direction. The toughness Γ was calculated by integrating the stress-stretch curve of the unnotched sample from $\lambda = 1$ to the critical stretch $\lambda = \lambda_c$ to get $W(\lambda_c)$, and then multiplied by the sample height H, i.e., $\Gamma = HW(\lambda_c)$. The adhesion energy was calculated as twice the value of the plateau peeling force F divided by the sample width w, which equaled to $2F/w$. The sample size for the pure-shear test was set to be 40 mm × 100 mm in order to clearly observe the fracture process. The sample size for the fatigue test was 20 mm × 100 mm. For each applied stretch $\lambda_{applied}$, we conducted cyclic test for both the unnotched sample and notched sample. The stress-stretch curve of the unnotched sample was adopted to calculate the energy release rate G. The formula is the same as that for calculating the toughness. The fracture process of the notched sample was recorded by a digital camera (Cannon GI 890). We recorded the critical cycle number N when the first hard fiber totally broke at the front of the crack tip. By changing the energy release rate G, we can plot the G-N curve.

3. The threshold and toughness of elastomers

We collect data of threshold and toughness of various elastomers from published papers (Ahagon and Gent, 1975; Bhowmick, 1988; Fleck et al., 1994; Gent and Tobias, 1982; Lake, 1972, 1995; Lake and Thomas, 1967) (Fig. 1). Existing elastomers have high toughness on the order of $10^3 \sim 10^5$ J/m^2, but the threshold is much lower than the toughness. For instance, natural rubber shows a toughness of ~10,000 J/m^2, but the threshold is only ~50 J/m^2 (Lake and Thomas, 1967). For other elastomers such as chloroprene rubber, butadiene rubber and polydimethylsiloxane (PDMS), the threshold is on the same order, irrelevant of the type of elastomers. The low fatigue threshold for all elastomers is understood in terms of the classical Lake-Thomas model. At the fatigue threshold, the extension of crack no longer activates the bulk dissipation of the elastomer; only the breaking of polymer chains (covalent bonds) at the crack plane contributes to the energy release. Improving the fatigue threshold of elastomers has become a long standing issue for decades, but less progress has been reported. Very recently, Wang et al. have proposed a strategy to prepare PDMS composite to achieve a threshold of 160 J/m^2 (Wang et al., 2019), while the stretchability of this composite is poor. Threshold above 1000 J/m^2 has been reported for the PVA hydrogels (Lin et al., 2019a, 2019b), and for an elastomer/hydrogel composite (Xiang et al., 2019). In this paper, we have achieved a high threshold of 500 J/m^2 for highly stretchable composite elastomer, one order of magnitude higher than existing elastomers.

It is noted that a high threshold tearing energy of 200~1100 J/m^2 has been reported for carbon black filled rubbers (Bhowmick et al., 1983, 1990). However, the threshold was determined under static threshold conditions; i.e., the static tearing tests at high temperature, low rates of tearing, and with swollen samples. They had not conducted cyclic fatigue tests. We call the threshold under static tearing tests the slow-crack threshold and the threshold under cyclic tests the fatigue-crack threshold. In literature, it has been unclear whether the fatigue-crack threshold and the slow-crack threshold are identical (Bai et al., 2019a). Therefore, we just collected the data of fatigue-crack thresholds in Fig. 1.

4. Classical Lake-Thomas model and the generalized Lake-Thomas model

The high threshold of the composite elastomer can be explained by the generalized Lake-Thomas model established here, where macroscopic fibers rather than polymer chains are broken to advance the crack. Since the elastic energy stored in macroscopic fibers is much higher than that of polymer chains, the energy needed for the propagation of the crack is also much higher.

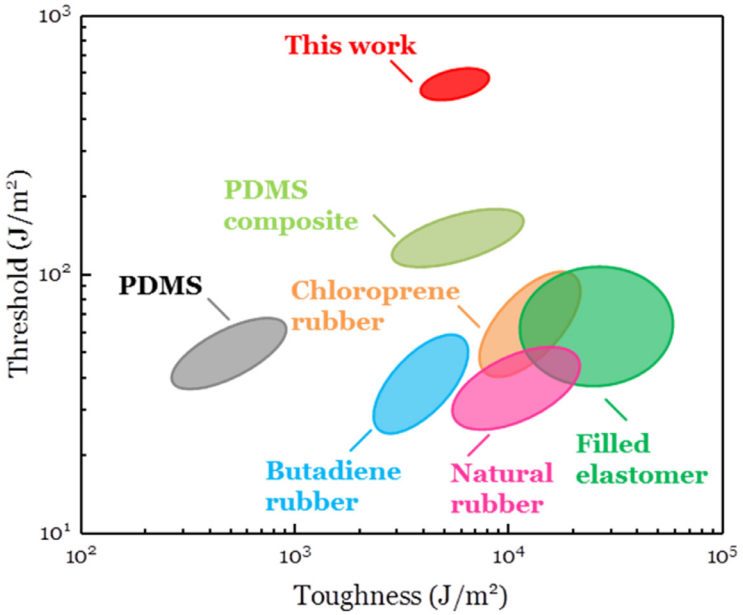

Fig. 1. The threshold and toughness of various elastomers. Existing elastomers have high toughness on the order of $10^3 \sim 10^5$ J/m^2, whereas their fatigue thresholds are only ~50 J/m^2. The stretchable composite elastomers in this paper demonstrate an extraordinarily high threshold of 500 J/m^2, one order of magnitude higher than existing elastomers. The collected materials include natural rubber, chloroprene rubber, butadiene rubber and polydimethylsiloxane (PDMS). PDMS composite refers to a composite of hard PDMS and soft PDMS (Wang et al., 2019).

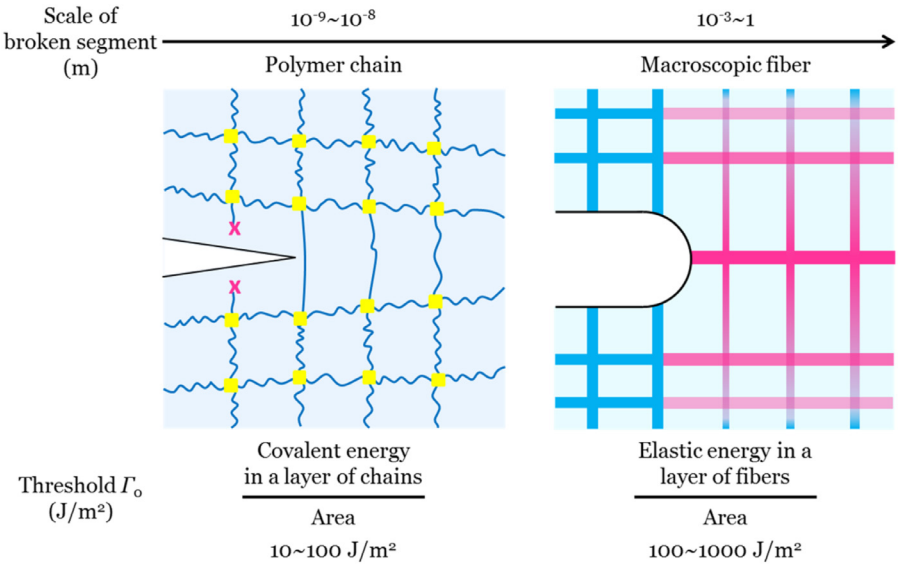

Fig. 2. Comparison of the classical Lake-Thomas model and the generalized Lake-Thomas model. (a) The classical Lake-Thomas model assumes that a crack propagates by breaking only a single layer of chains across the crack plane. Thus the fatigue threshold is equal to the covalent energy stored in a layer of polymer chains per unit area (10~100 J/m^2). (b) The composite elastomers consist of hard elastomer fiber and soft elastomer matrix. In the generalized Lake-Thomas model, the crack extends by breaking the hard fibers and the threshold is equal to the elastic energy stored in a layer of fibers per unit area. Since the energy stored in a macroscopic fiber is essentially higher than that of polymer chains, the fatigue threshold can be simply enhanced to 100~1000 J/m^2.

The schematic for classical Lake-Thomas model is shown (Fig. 2). Elastomer is a three-dimensional polymer network. Each polymer chain consists of a large number of monomers linked by strong covalent bonds. Polymer chains are crosslinked to form a network also by covalent bonds. Between the chains, molecules interact through weak physical bonds, such as hydrogen bonds and van der Waals interaction. Lake-Thomas model assumes that the energy needed to advance the crack per unit area in a homogeneous elastomer equals to the covalent energy of a layer of polymer chains per unit area. This gives the equation $\Gamma_0 = el$, where e is the chemical energy per unit volume, and l is the thickness of the single-chain layer

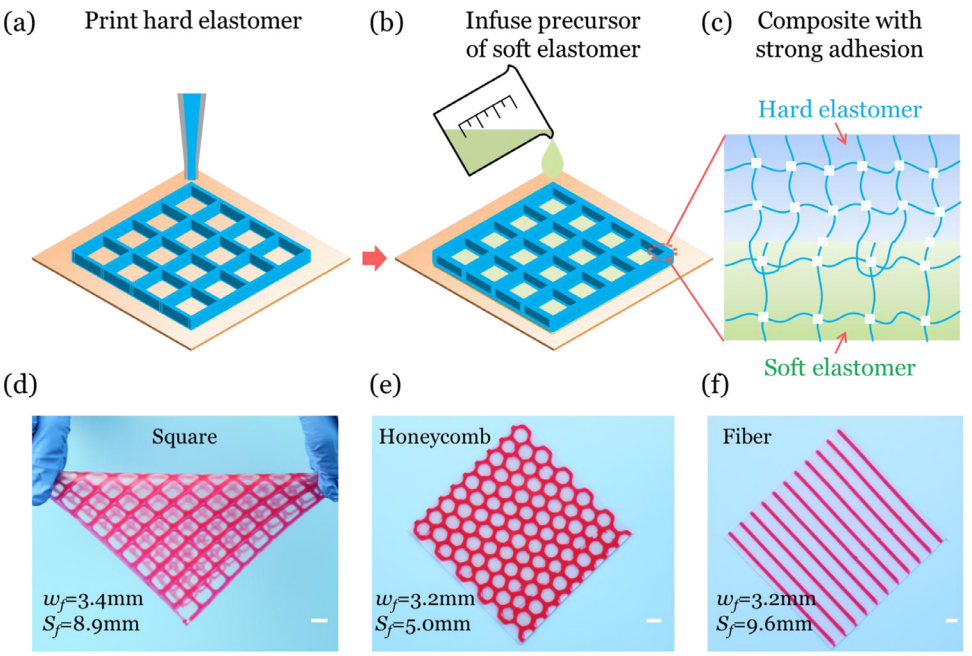

Fig. 3. Manufacture of composite elastomers. (a) A designed pattern of the hard elastomer is printed on a hot platform ($T = 110\,°C$) to initiate the fast polymerization. The printed hard elastomer is further cured in an oven at 60 °C for 4 h. (b) The precursor of the soft matrix is infused into a mold to fill the space left by the printed pattern. The composite is preserved at room temperature for 12 h to cure the soft matrix. (c) Once cured, the soft elastomer and the hard elastomer will form strong adhesion at the interface. The designed patterns include (d) 2D square, (e) 2D honeycomb and (f) 1D parallel lines. The red part is hard elastomer and the white part is soft elastomer. w_f is the average width of a single fiber; S_f is the average spacing between two single fibers for 2D square and 1D composites, or the side length of the internal hexagon for the 2D honeycomb composite. Scale bar, 1 cm.

in the undeformed state. The energy per unit volume is $e = bJ$, where b is the number of single bonds per unit volume, J is the chemical energy of a C–C bond. In the undeformed state, the thickness of the single-chain layer is estimated by the random-walk model: $l = an^{1/2}$, where a is the length of the monomer and n is the number of monomers in the chain. Combining the above equations we can get:

$$\Gamma_0 = Jabn^{1/2} \tag{1}$$

We take the numbers from the original paper of G. J. Lake and A. G. Thomas: $J = 3.3 \times 10^{-19}$ J, $a = 4.6 \times 10^{-10}$ m, and $bn^{1/2} = 6.6 \times 10^{28}/\text{m}^3$. The Lake-Thomas model gives $\Gamma_0 = 10\,\text{J/m}^2$. Here we omit possible numerical pre-factors.

For the composite elastomers, we propose a generalized Lake-Thomas model to predict the threshold. Analogically, the energy needed to advance the crack per unit area equals to the covalent energy of a layer of fibers per unit area. This mechanism gives the following equation:

$$\Gamma_0 = LMU \tag{2}$$

where L is the length of the fiber element, M is the number of fiber elements per unit volume and U is the energy needed to break the fiber.

For a fiber reinforced composites, the length of the fiber is on the order of cm, thus $L = 1 \times 10^{-2}$ m. Consider a cube with a side length of L. The cube has a volume of $V = L^3$ and has 3 independent edges. Then M can be well estimated by $3/V$ as $M = 3 \times 10^6\,\text{m}^{-3}$. The deformation in the fiber is assumed to be uniaxial. Then we can estimate U from the uniaxial tension test: the fiber typically breaks at $\lambda = 3$, thus by integrating the stress-stretch curve of uniaxial tension from $\lambda = 1$ to $\lambda = 3$, we obtain $U = 0.0133$ J. The generalized Lake-Thomas model gives a threshold of $\Gamma_0 = 399\,\text{J/m}^2$.

The essential reason for the low threshold of elastomers is that the energy needed to break polymer chains is small. Since the energy stored in a macroscopic fiber is much higher than that of polymer chains, the fatigue threshold can be simply enhanced for the composite.

5. Manufacture of the composite elastomers

Here we demonstrate the method to manufacture the composite elastomers (Fig. 3). The composite elastomer consists of elastomer fiber with a high modulus (hard elastomer) and elastomer matrix with a low modulus (soft elastomer). The first step is to print a hard elastomer. The precursor of the hard elastomer is loaded into a syringe of a direct-ink-writing

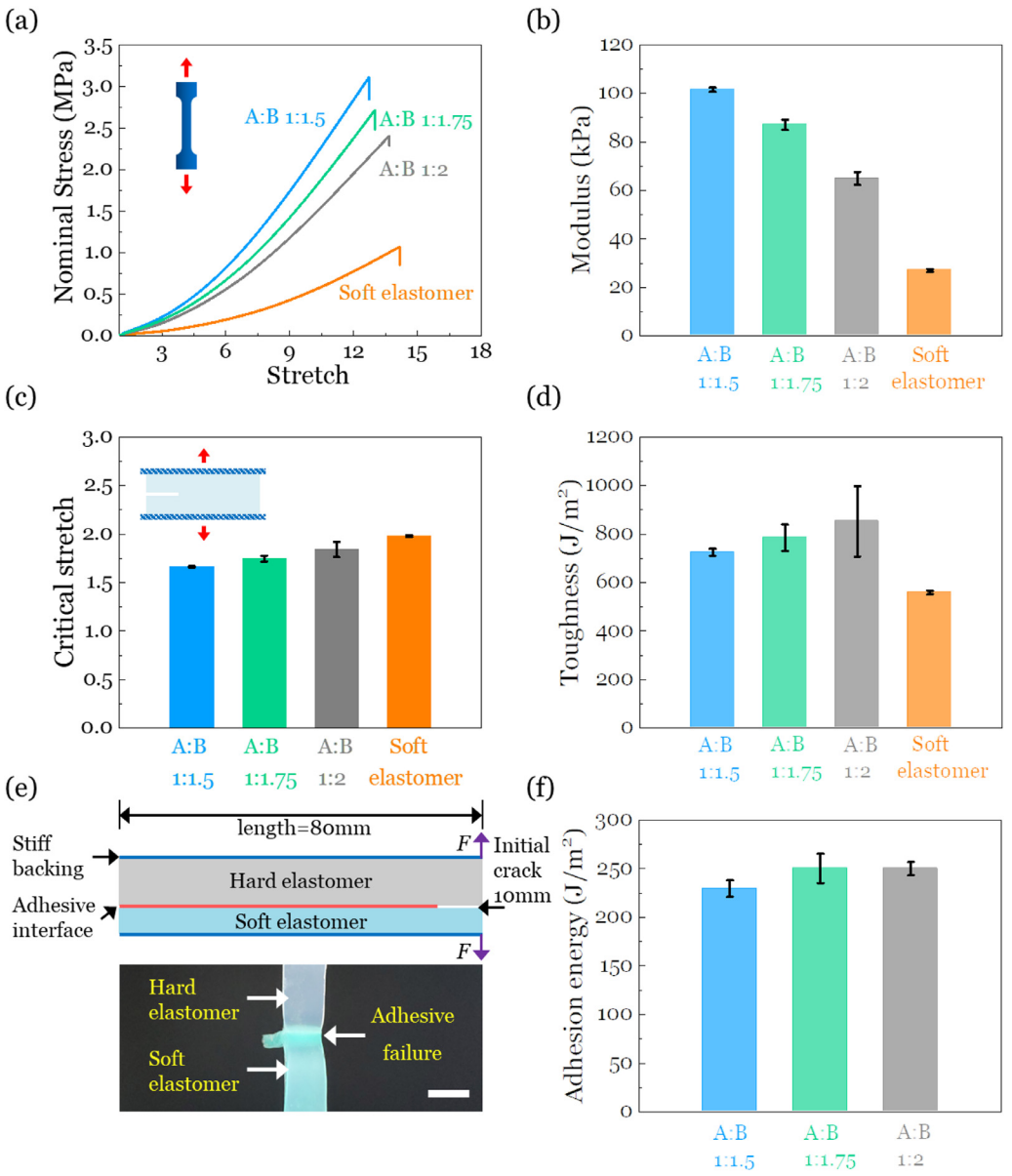

Fig. 4. Mechanical properties of homogenous elastomers. Soft elastomer used here is Ecoflex. Hard elastomers are prepared by mixing part A (Dragon skin-0020) and part B (Ecoflex-0030) in various weight ratios. (a) Uniaxial tension curves of various hard and soft elastomers. All the elastomers show high stretchability (ultimate stretch>12). (b) Young's moduli of hard and soft elastomers. The highest modulus for the hard elastomer is 101.44 ± 0.87 kPa, while the soft elastomer shows a modulus of 26.97 ± 0.63 kPa. (c) Critical stretch λ_c of the notched pure-shear samples for hard and soft elastomers. (d) Toughness of hard and soft elastomers. (e) Schematic of the 180-degree peeling test and the observed adhesive failure mode in peeling tests. (f) Adhesion energy of various hard elastomers to the soft elastomer. All cases demonstrate high adhesion energy beyond 200 J/m^2. Scale bar, 1 cm.

printer. Meanwhile, the metal platform of the printer is pre-heated to 110 °C. Driven by the air pressure, the precursor flows from the nozzle to the platform in a designed 2D pattern. The hot platform initiates the fast polymerization of the hard elastomer (Fig. 3a). The printed hard elastomer is further cured in an oven at 60 °C for 4 h to complete the polymerization. Next, the precursor of the soft elastomer is infused into the mold to fill the space left by the patterned hard elastomer (Fig. 3b). The composite is stored at room temperature for 12 h to cure the soft matrix. Finally, the soft elastomer and the hard elastomer form strong adhesion at the interface, as a result of the covalent interlinking and topological entanglement (Fig. 3c). With the help of 3D printing technology, we can easily print 2D patterned composites such as square (Fig. 3d) and honeycomb (Fig. 3e), and 1D fiber reinforced composites (Fig. 3f). The red part is hard elastomer and the white part is soft elastomer.

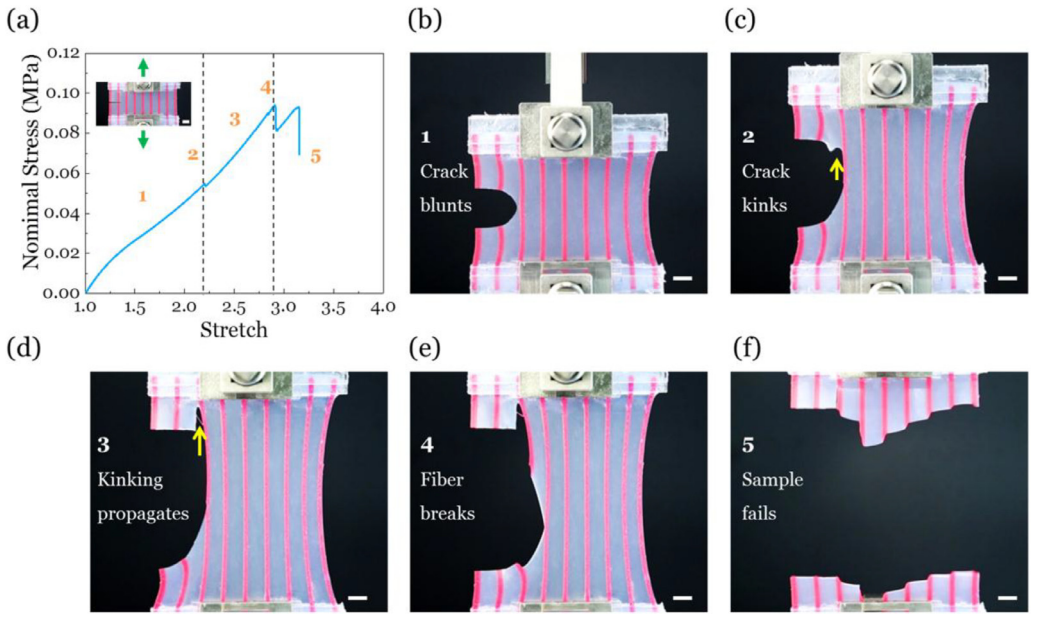

Fig. 5. Fracture process of 1D composites. (a) The stress-stretch curve for the notched composite reinforced by 1D hard fibers. The curve is divided into 5 regions corresponding to the fracture process. Scale bar, 1 cm. (b) The crack blunts at the tip, enabling the hard elastomer to be stretched over a long segment. (c) The crack kinks to the vertical direction along the interface. (d) The kinking crack keeps propagating to the clamp. (e) The hard fiber breaks at a large stretch and the stored elastic energy is released. (f) The sample totally fails and all fibers are broken. Scale bar, 1 cm.

6. Mechanical measurements of homogenous elastomers

Two prerequisites should be satisfied for the synthesis of the composite: (1) the hard elastomer and soft elastomer need to have large modulus difference; (2) the interface between the hard elastomer and soft elastomer should be strong to resist the shear deformation. To validate these two conditions, we will characterize the mechanical properties of the homogeneous elastomers in this section. The measured mechanical properties include the uniaxial tension curves, Young's modulus, toughness and adhesion energy.

We mix Dragon skin-0020 A and Ecoflex-0030 B in various weight ratios to synthesize hard elastomers with different modulus. We mix part A and part B of Ecoflex-0030 to synthesize the soft elastomer. The uniaxial tension curves of various elastomers are plotted (Fig. 4a). The higher the ratio of (Ecoflex-0030 B), the lower the stress at the same stretch. All the elastomers show extremely high stretchability (ultimate stretch>12). We can obtain Young's modulus of these elastomers by linearly fitting the stress-stretch curves from $\lambda = 1$ to $\lambda = 2.5$ (Fig. 4b). Higher fraction of (Ecoflex-0030 B) leads to a lower modulus for the composite. The largest modulus ratio is 3.76 between the hard elastomer (A:B = 1:1.5) to the soft elastomer. The modulus ratio can be easily tuned by adjusting the weight ratios between the two elastomer constituents. We further conduct pure-shear tests to determine the toughness of the elastomers. All notched samples show similarly low critical stretch with $\lambda_c < 2$ (Fig. 4c). The toughness Γ is calculated by integrating the stress-stretch curve of the unnotched sample from $\lambda = 1$ to $\lambda = \lambda_c$ to get $W(\lambda_c)$ and then multiplied by the sample height H, i.e., $\Gamma = HW(\lambda_c)$. The hard elastomers show similar toughness $\sim 800\,\mathrm{J/m^2}$, slightly higher than that of soft elastomer ($558.67 \pm 8.33\,\mathrm{J/m^2}$) (Fig. 4d). Since strong adhesion between the two elastomer constituents is significant to the integrity of the composites (Wang et al., 2019), we will characterize the adhesion energy using 180-degree peeling test (Fig. 4e). We prepare bilayer samples of the hard elastomer and soft elastomer, and glue stiff PET backing to the upper and lower faces of the bilayer to constrain the elongation of the peeling arm (Yang et al., 2018). An initial crack of 10 mm is made on the interface. We observe adhesive failure for all the peeling samples (Fig. 4e), where the white one is the hard elastomer and the green one is the soft elastomer. High adhesion energy can be achieved for all the three hard elastomers to soft elastomer without any chemical treatment (Fig. 4f). The adhesion energy are $230 \pm 8\,\mathrm{J/m^2}$, $250 \pm 15\,\mathrm{J/m^2}$ and $250 \pm 7\,\mathrm{J/m^2}$ for the cases of A:B (1:1.5), A:B (1:1.75) and A:B (1:2), respectively. In all the following experiments, we will use the elastomer with a weight ratio of (A:B = 1:1.5) as the hard elastomer, because of its largest modulus.

7. Fracture of composite elastomers

To compare the fracture process of 1D and 2D composites, we use a large sample (width = 100 mm, height = 40 mm) to observe the crack propagation. We firstly study the 1D fiber reinforced composites with an initial cut of 20 mm. The parallel hard fibers are evenly distributed in the soft matrix. The notched sample is continuously loaded till the ultimate rupture and

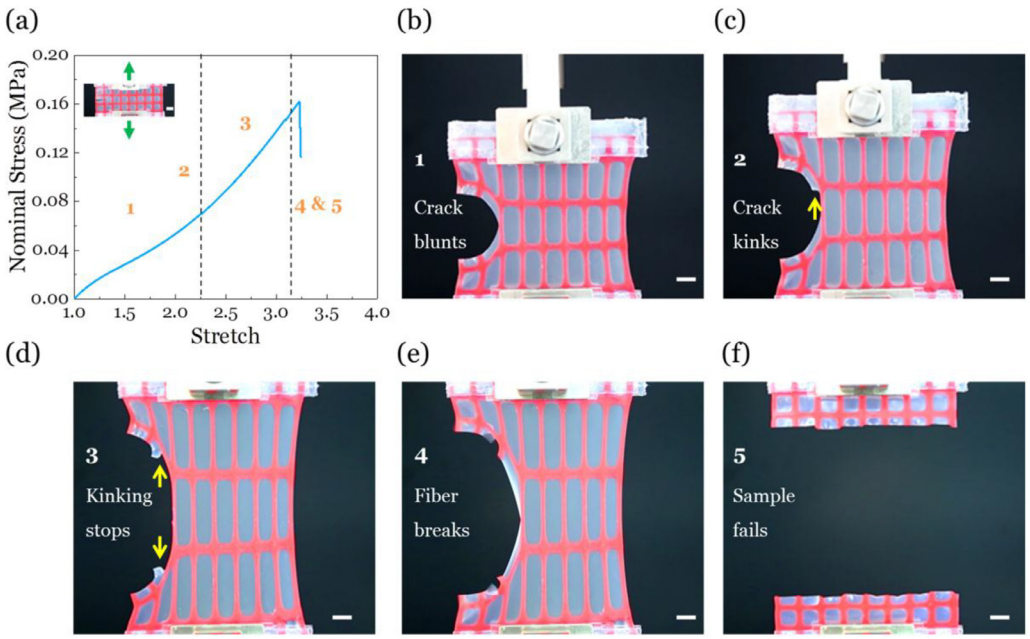

Fig. 6. Fracture process of 2D composites. (a) The stress-stretch curve for the notched composite with 2D distributed hard fibers. The curve is divided into 5 regions corresponding to the fracture process. Scale bar, 1 cm. (b) The crack blunts at the tip, enabling the hard elastomer to be stretched. (c) The crack kinks to the vertical direction along the interface. (d) The kinking crack stops at the edge of the horizontal fibers. (e) The hard fiber breaks at a large stretch and the stored elastic energy is released. (f) The notched sample fails finally. Scale bar, 1 cm.

the stress-stretch curve is recorded (Fig. 5a). The curve is divided into 5 regions corresponding to the 5 stages in the fracture process. Firstly, the crack propagates smoothly in the soft matrix to the edge of the hard fiber and blunts greatly due to low modulus of the soft matrix (Fig. 5b). Secondly, the crack kinks to the vertical direction along the interface (Fig. 5c). The stress concentration in the hard fiber at the crack tip is significantly reduced due to the crack blunting. The alleviated stress concentration around the hard fiber enables it to be stretched over a long segment and a large amount of elastic energy is stored in the fiber. Thirdly, the kinking crack keeps propagating along the interface through the whole sample and stops at the clamp (Fig. 5d). Fourthly, the hard fiber breaks at a large stretch and the stored elastic energy is released, leading to a sudden drop of the stress (Fig. 5e). Since the remaining intact fibers can still bear load, the stress goes up again. Finally, the whole sample fails and all fibers are broken (Fig. 5f).

Although the parallel alignment of 1D hard fibers can increase the toughness and the threshold, the kinking crack will split the whole sample before the breaking of the fibers. The crack kinking should be blocked rather than propagates through the whole sample. This failure mode should be avoided for practical applications such as biomedical devices, soft robots (Martinez et al., 2014) and wearable electronics.

As comparison, we will show the fracture process of the composite with 2D patterned fibers (Fig. 6). The hard fibers are continuously distributed in the soft matrix in both the vertical and horizontal direction. The stress-stretch curve is shown (Fig. 6a). Similarly, we also divide the fracture process into 5 stages. The crack also blunts and kinks to the vertical direction along the interface (Fig. 6b and c). However, different to the 1D case, the kinking crack propagation will be blocked by the horizontal fiber (Fig. 6d). Further stretch leads to the breaking of the hard fiber and the failure of the whole sample (Fig. 6e and f). 2D aligned hard fibers can not only increase the toughness and threshold, but also constrain the crack kinking in a single grid before the fiber breaking.

The toughness of the soft elastomer, hard elastomer, 1D and 2D composites are compared (Fig. 7). The samples are set to be 100 mm in width and 40 mm in height for the pure shear test. Firstly, unnotched samples of various materials are stretched monotonously until failure. Composites rupture at almost the same stretch as homogeneous elastomers, and they all show a large ultimate stretch with $\lambda > 5$ (Fig. 7a). Secondly, notched samples with a cut of 20 mm are stretched until the final rupture. Composites show much larger critical stretch λ_c than homogeneous elastomers (Fig. 7b). Local damage (such as fiber breaking) may occur before reaching the peak stress, implied by the stress drop for 1D composite. Here we omit this detail and regard the peak stress as the fracture point (marked with the symbol "×" in stress-stretch curves) to calculate the toughness. The critical stretch λ_c of notched samples are 1.52 ± 0.02, 1.43 ± 0.01, 3.11 ± 0.22 and 3.06 ± 0.19, for soft elastomer, hard elastomer, 1D and 2D composites, respectively (Fig. 7c). Corresponding toughness are $305.33 \pm 18.04\,J/m^2$, $617.33 \pm 23.09\,J/m^2$, $5421.33 \pm 1281.53\,J/m^2$ and $5693.33 \pm 1194.43\,J/m^2$ for soft elastomer, hard elastomer, 1D and 2D composites, respectively (Fig. 7d). It is seen that the fiber reinforced composite strategy can greatly toughen the homogeneous elastomers by an order of magnitude.

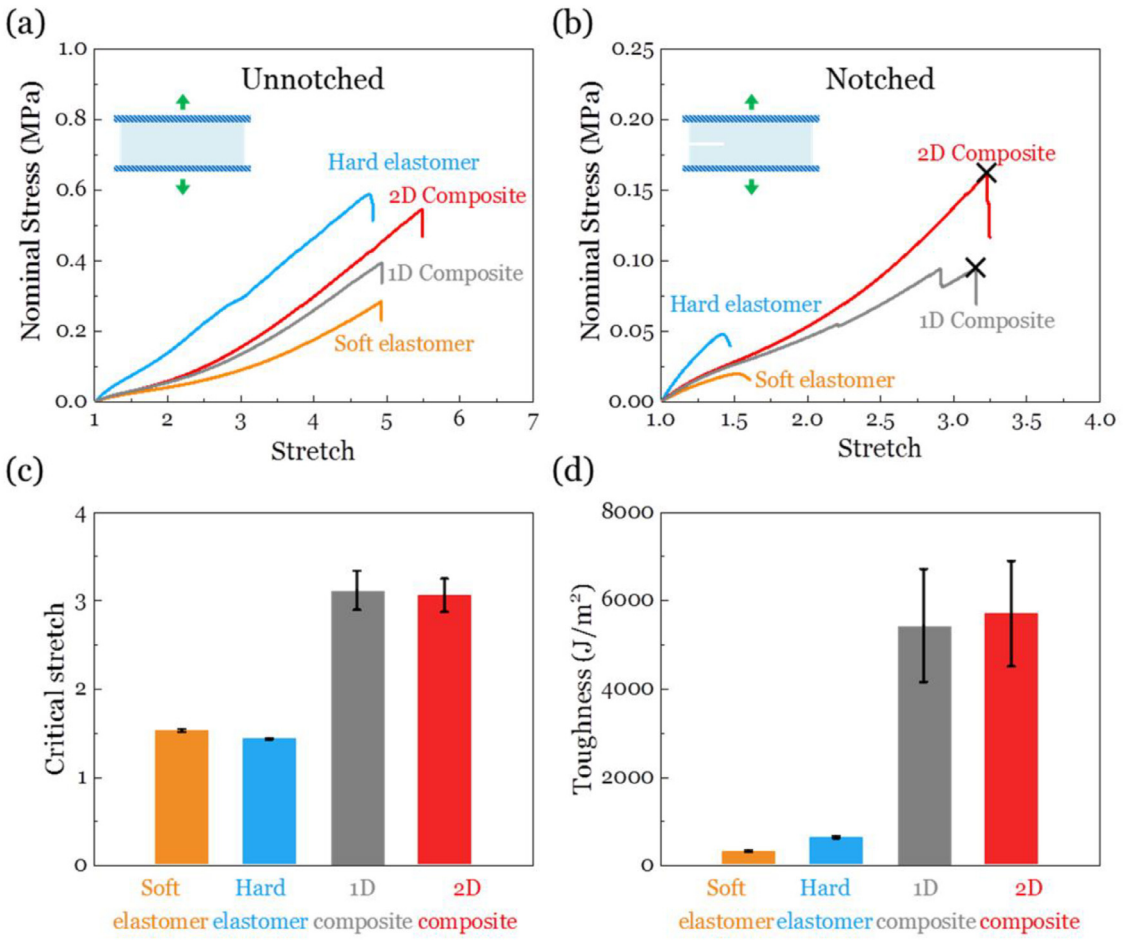

Fig. 7. Fracture properties of homogeneous elastomers and composite elastomers. The stress-stretch curves for the unnotched samples (a) and notched samples (b). All the unnotched samples rupture at almost the same stretch, while the notched composite elastomers rupture at a much larger stretch than homogeneous elastomers. (c) The critical stretch of notched samples. (d) The toughness of 1D, 2D composites can reach ~6000 J/m^2, an order of magnitude higher than that of homogeneous elastomer.

8. Fatigue of 2D composite elastomers

To determine the fatigue resistance of the composite elastomers, we carry out cyclic pure-shear tests following the procedure developed by Thomas A. G. and others (Tang et al., 2017; Thomas, 1959). The definition of fatigue failure corresponds to the failure of the first hard fiber in front of the initial crack. The cyclic test of the notched sample is used to quantify the crack growth, while that of the unnotched sample is used to calculate the energy release rate G from stress-stretch curves. The notched sample is stretched from $\lambda = 1$ to $\lambda = \lambda_{applied}$ repeatedly at a frequency of $f = 0.2$ Hz (Fig. 8a). The unnotched sample is also stretched to the same displacement repeatedly at the same frequency. Since the stress-stretch curves demonstrate steadily slight decline with cycles, it is necessary to determine which curve to be integrated to obtain $G = HW(\lambda_{applied})$ (Fig. 8b). Following our previous papers (Bai et al., 2017; Zhang et al., 2018), we use the 2000th cycle to calculate G, since the stress decline is negligible after 2000 cycles (Fig. 8b). While for some large stretches, the notched sample will fail locally before 2000 cycles. In this case, we define N_c as the cycle number when the first fiber totally breaks and use the N_c^{th} cycle of stress-stretch curve to calculate G.

We observe four failure modes of the composite elastomers at different loadings: catastrophic fracture, fiber cut by crack, crack kinks and fiber breaks, and crack stopped by fibers. When the applied stretch is high ($\lambda = 3.1$, $G = 3130$ J/m^2), the sample fails catastrophically at the 1st cycle (Fig. 8c). We lower the stretch slightly ($\lambda = 2.75$ and $G = 1700$ J/m^2), the crack propagates and cuts the fiber directly after 60 cycles (Fig. 8d). We further reduce the stretch to ($\lambda = 2.25$ and $G = 1068$ J/m^2), the crack kinking first occurs at the 50th cycles. After 478 cycles, the fiber breaks (Fig. 8e). When the stretch is reduced to a low level such as ($\lambda = 2$ and $G = 537$ J/m^2), crack kinking will happen first (kinking starts at the 117th cycle and stops at the 460th cycle), but the crack is fully stopped by the hard fiber even after 39,200 cycles (Fig. 8f). In fact, the sample can

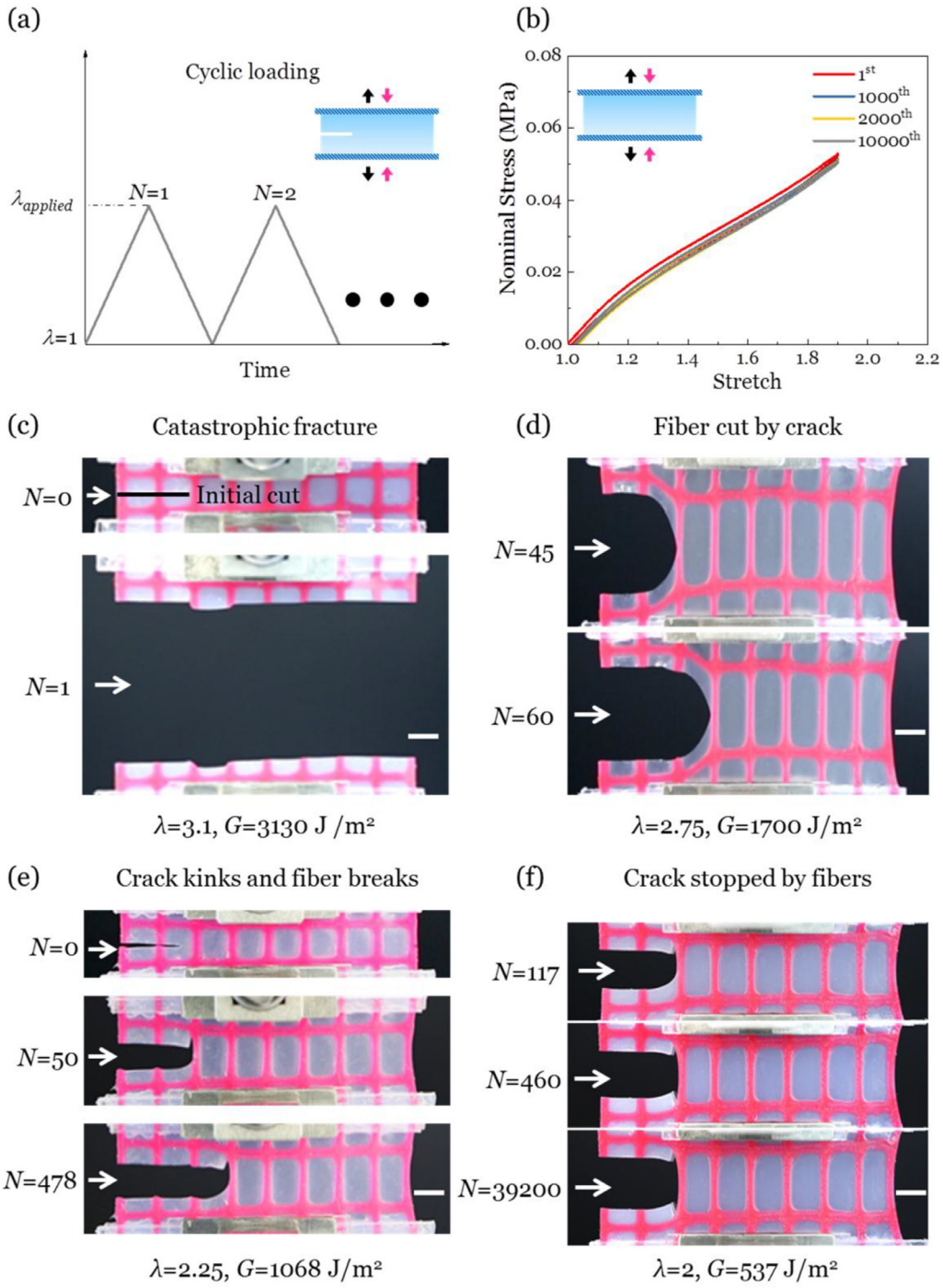

Fig. 8. Fatigue test of the composite elastomer. (a) The notched sample is stretched from $\lambda = 1$ to $\lambda = \lambda_{applied}$ repeatedly. When the first fiber breaks, we regard the sample as damaged and record the critical cycle number N_c. (b) The unnotched sample is also stretched from $\lambda = 1$ to $\lambda = \lambda_{applied}$ repeatedly for the calculation of the energy release rate G. (c) When $\lambda = 3.1$, $G = 3130\,\mathrm{J/m^2}$, the sample fails at the first cycle. (d) When $\lambda = 2.75$, $G = 1700\,\mathrm{J/m^2}$, the first fiber breaks directly after 60 cycles. (e) When $\lambda = 2.25$, $G = 1068\,\mathrm{J/m^2}$, the crack kinks at the interface at the 50th cycle and the fiber breaks at the 478th cycles. (f) When $\lambda = 2$, $G = 537\,\mathrm{J/m^2}$, the crack kinking starts at the 117th cycle and stops at the 460th cycle, but the fiber does not break even after 39,200 cycles. This energy release rate G is the lower limit of the fatigue threshold.

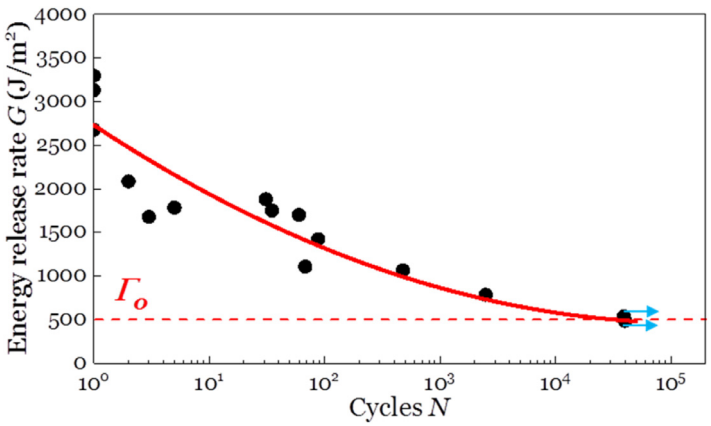

Fig. 9. *G-N* curve of the composite elastomer. At each energy release rate *G*, we record the critical cycle number *N* when the first fiber breaks and plot the *G-N* curve. As *G* decreases, the cycle number of the composite increases dramatically; around the fatigue threshold Γ_0, the cycle number is ~40,000 cycles which we regard as infinity. This *G-N* curve gives a lower limit of the fatigue threshold of 500 J/m^2, ten times of that for natural rubbers.

be loaded at this stretch for more cycles, but we have not pursued that due to the limitation of time. We regard this energy release rate $G = 537$ J/m^2 as the lower limit of the fatigue threshold for the 2D composites.

Usually at room temperature, it is difficult to achieve threshold strength. Threshold strength is obtained when all dissipative processes are minimized, by doing experiments at high temperature, low-rates tearing and under swollen conditions (Bhowmick et al., 1983; Gent and Tobias, 1982). In our experiments, we determine the fatigue threshold at room temperature, which may be higher than that under threshold conditions. Hence, the fatigue threshold here means the minimum value in this experiment.

We record each energy release rate *G* and the corresponding failure cycle number *N* to plot the *G-N* curve (Fig. 9). We regard the first fiber breaking as the failure of the sample. A clear declining trend is seen for the *G-N* curve: the lower the applied load *G*, the longer the sustained cycle *N*. When *G* approaches a threshold Γ_0, the cycle number *N* goes up dramatically. The blue arrows mean that after tens of thousands cycles, the sample still remain intact. When $G = 537$ J/m^2, the cycle number is ~40,000 cycles which we regard as infinity. We could do more cycles near the threshold, but we did not pursue that here. This *G-N* curve gives a fatigue threshold of ~500 J/m^2, one order of magnitude higher than that of natural rubbers (50 J/m^2).

9. Conclusion

In conclusion, we have developed fatigue-resistant elastomers. The fatigue threshold for the composite elastomer is beyond 500 J/m^2, one order of magnitude higher than existing elastomers. The threshold of the composites has been predicted by a generalized Lake-Thomas model. We have printed several 2D patterns of hard fibers to synthesize the composite. The 2D composite elastomers demonstrate different fracture process to that of 1D composites and four failure modes are shown in their fatigue tests: catastrophic fracture, fiber cut by crack, crack kinks and fiber breaks, and crack stopped by fibers. Recent study has shown that network imperfections can reduce the strength of synthesized polymers by 5 orders of magnitude (Liu et al., 2019; Yang et al., 2019a). It is worthwhile to develop high-strength fibers for composites. Moreover, 3D patterns of hard fibers can be printed to mimic biological tissues in the future work. We hope that this work can stimulate more fundamental research and engineering applications.

Declaration of Competing Interest

None.

Acknowledgements

J.D. Tang acknowledges the support of National Natural Science Foundation of China (No. 11702208), and the Program for Postdoctoral Innovative Talents (No. BX201700192). Z.G. Suo acknowledges the support of Harvard University MRSEC (DMR-14-20570).

References

Ahagon, A., Gent, A., 1975. Threshold fracture energies for elastomers. J Polym Sci 13, 1903–1911.
Bai, R., Chen, B., Yang, J., Suo, Z., 2019a. Tearing a hydrogel of complex rheology. J Mech Phys Solids 125, 749–761.
Bai, R., Yang, J., Morelle, X.P., Suo, Z., 2019b. Flaw - insensitive hydrogels under static and cyclic loads. Macromol Rapid Commun 40, 1800883.

Bai, R., Yang, Q., Tang, J., Morelle, X.P., Vlassak, J., Suo, Z., 2017. Fatigue fracture of tough hydrogels. Extreme Mech Lett 15, 91–96.
Berisio, R., Vitagliano, L., Mazzarella, L., Zagari, A., 2002. Crystal structure of the collagen triple helix model [(Pro-Pro-Gly) 10] 3. Protein Sci 11, 262–270.
Bhowmick, A., Gent, A., Pulford, C., 1983. Tear strength of elastomers under threshold conditions. Akron Univ OH Inst of Polymer Science.
Bhowmick, A.K., 1988. Threshold fracture of elastomers. Polym Rev 28, 339–370.
Bhowmick, A.K., Neogi, C., Basu, S., 1990. Threshold tear strength of carbon black filled rubber vulcanizates. J Appl Polym Sci 41, 917–928.
Bhowmick, A.K., Stephens, H., 2000. Handbook of elastomers. CRC Press.
Creton, C., Ciccotti, M., 2016. Fracture and adhesion of soft materials: a review. Rep Prog Phys 79, 046601.
Fleck, N., Kang, K., Ashby, M., 1994. Overview no. 112: the cyclic properties of engineering materials. Acta Metall Mater 42, 365–381.
Gent, A.N., 2012. Engineering with rubber: how to design rubber components. Carl Hanser Verlag GmbH Co KG.
Gent, A.N., Tobias, R., 1982. Threshold tear strength of elastomers. J Polym Sci 20, 2051–2058.
Ilievski, F., Mazzeo, A.D., Shepherd, R.F., Chen, X., Whitesides, G.M., 2011. Soft robotics for chemists. Angew Chem Int Ed 50, 1890–1895.
Jurvelin, J., Buschmann, M., Hunziker, E., 2003. Mechanical anisotropy of the human knee articular cartilage in compression. Proc Inst Mech Eng Part H 217, 215–219.
Kim, D.-H., Lu, N., Ma, R., Kim, Y.-S., Kim, R.-H., Wang, S., Wu, J., Won, S.M., Tao, H., Islam, A., 2011. Epidermal electronics. Science 333, 838–843.
Lake, G., 1972. Mechanical fatigue of rubber. Rubber Chem Technol 45, 309–328.
Lake, G., 1995. Fatigue and fracture of elastomers. Rubber Chem Technol 68, 435–460.
Lake, G., Thomas, A., 1967. The strength of highly elastic materials. Proc R Soc London Ser A 300, 108–119.
Launey, M.E., Buehler, M.J., Ritchie, R.O., 2010. On the mechanistic origins of toughness in bone. Annu Rev Mater Res 40, 25–53.
Le Floch, P., Meixuanzi, S., Tang, J., Liu, J., Suo, Z., 2018. Stretchable seal. ACS Appl Mater Interfaces 10, 27333–27343.
Lin, S., Liu, J., Liu, X., Zhao, X., 2019a. Muscle-like fatigue-resistant hydrogels by mechanical training. Proc Natl Acad Sci 116, 10244–10249.
Lin, S., Liu, X., Liu, J., Yuk, H., Loh, H.-C., Parada, G.A., Settens, C., Song, J., Masic, A., McKinley, G.H., 2019b. Anti-fatigue-fracture hydrogels. Sci Adv 5 eaau8528.
Liu, J., Yang, C., Yin, T., Wang, Z., Qu, S., Suo, Z., 2019. Polyacrylamide hydrogels. II. Elastic dissipater. J Mech Phys Solids, 103737.
Liu, Q., Nian, G., Yang, C., Qu, S., Suo, Z., 2018. Bonding dissimilar polymer networks in various manufacturing processes. Nat Commun 9, 846.
Long, R., Hui, C.-Y., 2015. Crack tip fields in soft elastic solids subjected to large quasi-static deformation—a review. Extreme Mech Lett 4, 131–155.
Mannsfeld, S.C., Tee, B.C., Stoltenberg, R.M., Chen, C.V.H., Barman, S., Muir, B.V., Sokolov, A.N., Reese, C., Bao, Z., 2010. Highly sensitive flexible pressure sensors with microstructured rubber dielectric layers. Nat Mater 9, 859.
Mars, W., Fatemi, A., 2002. A literature survey on fatigue analysis approaches for rubber. Int J Fatigue 24, 949–961.
Martin, O.R., 1959. Molded rubber football. Google Patents.
Martinez, R.V., Glavan, A.C., Keplinger, C., Oyetibo, A.I., Whitesides, G.M., 2014. Soft actuators and robots that are resistant to mechanical damage. Adv Funct Mater 24, 3003–3010.
Merritt, D., Weinhaus, F., 1978. The pressure curve for a rubber balloon. Am J Phys 46, 976–977.
Ritchie, R.O., 2014. Natural materials: armoured oyster shells. Nat Mater 13, 435.
Rogers, J.A., Someya, T., Huang, Y., 2010. Materials and mechanics for stretchable electronics. Science 327, 1603–1607.
Shepherd, R.F., Ilievski, F., Choi, W., Morin, S.A., Stokes, A.A., Mazzeo, A.D., Chen, X., Wang, M., Whitesides, G.M., 2011. Multigait soft robot. Proc Natl Acad Sci 108, 20400–20403.
Takeyama, T., Matsui, J., 1969. Recent developments with tire cords and cord-to-rubber bonding. Rubber Chem Technol 42, 159–256.
Tang, J., Li, J., Vlassak, J.J., Suo, Z., 2017. Fatigue fracture of hydrogels. Extreme Mech Lett 10, 24–31.
Thomas, A., 1959. Rupture of rubber. V. cut growth in natural rubber vulcanizates. Rubber Chem Technol 32, 477–489.
Wang, Z., Xiang, C., Yao, X., Le Floch, P., Mendez, J., Suo, Z., 2019. Stretchable materials of high toughness and low hysteresis. Proc Natl Acad Sci 116, 5967–5972.
Wegst, U.G., Bai, H., Saiz, E., Tomsia, A.P., Ritchie, R.O., 2015. Bioinspired structural materials. Nat Mater 14, 23.
Whanger, J.K., Harrall, S.J., 2004. Reinforced swelling elastomer seal element on expandable tubular. Google Patents.
Wiley, A.A., 1934. Rubber glove. Google Patents.
Xiang, C., Wang, Z., Yang, C., Yao, X., Wang, Y., Suo, Z., 2019. Stretchable and fatigue-resistant materials. Materials Today. https://doi.org/10.1016/j.mattod.2019.08.009.
Yang, C., Suo, Z., 2018. Hydrogel ionotronics. Nat Rev Mater 3, 125.
Yang, C., Yin, T., Suo, Z., 2019a. Polyacrylamide hydrogels. I. Network imperfection. J Mech Phys Solids 131, 43–55.
Yang, H., Li, C., Yang, M., Pan, Y., Yin, Q., Tang, J., Qi, H.J., Suo, Z., 2019b. Printing hydrogels and elastomers in arbitrary sequence with strong adhesion. Adv Funct Mater, 1901721.
Yang, J., Bai, R., Suo, Z., 2018. Topological adhesion of wet materials. Adv Mater 30, 1800671.
Yang, W., Sherman, V.R., Gludovatz, B., Schaible, E., Stewart, P., Ritchie, R.O., Meyers, M.A., 2015. On the tear resistance of skin. Nat Commun 6, 6649.
Zhang, W., Liu, X., Wang, J., Tang, J., Hu, J., Lu, T., Suo, Z., 2018. Fatigue of double-network hydrogels. Eng Fract Mech 187, 74–93.
Zhu, J., Stoyanov, H., Kofod, G., Suo, Z., 2010. Large deformation and electromechanical instability of a dielectric elastomer tube actuator. J Appl Phys 108, 074113.